

Log-Poisson cascade description of turbulent velocity-gradient statisticsM. Kholmyansky,¹ L. Moriconi,² R. M. Pereira,² and A. Tsinober^{1,3}¹*Faculty of Engineering, Tel Aviv University, Tel Aviv 69978, Israel*²*Instituto de Física, Universidade Federal do Rio de Janeiro, CP 68528, 21945-970 Rio de Janeiro, RJ, Brazil*³*Institute for Mathematical Sciences and Department of Aeronautics, Imperial College, London, 53 Princes Gate, Exhibition Road, South Kensington Campus, London SW7 2PG, United Kingdom*

(Received 15 June 2009; published 18 September 2009)

The Log-Poisson phenomenological description of the turbulent energy cascade is evoked to discuss high-order statistics of velocity derivatives and the mapping between their probability distribution functions at different Reynolds numbers. The striking confirmation of theoretical predictions suggests that numerical solutions of the flow obtained at low/moderate Reynolds numbers can play an important quantitative role in the analysis of experimental high Reynolds number phenomena, where small scales fluctuations are in general inaccessible from direct numerical simulations.

DOI: [10.1103/PhysRevE.80.036311](https://doi.org/10.1103/PhysRevE.80.036311)

PACS number(s): 47.27.nb, 47.27.Gs, 42.68.Bz

I. INTRODUCTION

Since the pioneering experimental work of Batchelor and Townsend, published exactly 60 years ago [1], it is known that scale-dependent Galilean invariant observables, such as velocity differences, fluctuate in a strongly non-Gaussian way at small scales in turbulent flows. This kind of statistical behavior, generally referred to as “intermittency,” indicates that the K41 picture of turbulence [2,3], which actually would correspond to the existence of a uniformly distributed energy dissipation field [4], should break down: a fact notoriously anticipated by Landau as early as in 1942 [5]. Not less remarkably, long before additional breakthrough experiments were performed [6], phenomenological models of the energy cascade advanced the conjecture that intermittency should be related to the stochastic multiplicative nature of the energy cascade process [7,8], implying that small scale strong fluctuations are, in some sense, fed by the weaker large scale ones.

The intermittency phenomenon is commonly associated with the anomalous scaling of velocity structure functions and those are relatively well described by schemes based on the multiplicative cascade idea [9]. Still, a comprehensive description dealing with both anomalous scaling and the non-Gaussian behavior of intermittent observables is a major challenge of three-dimensional turbulence theory [10]. Small scale strong fluctuations are believed to reflect the dynamics of coherent structures such as vortex filaments. Even though this is a markedly open problem, a similar physical picture is in fact well established in simpler contexts, as in Burgers turbulence [11], with shocks playing the role of “vortices.”

The log-Poisson model [12,13] yields perhaps the most intriguing description of the turbulent multiplicative cascade, since—as it is well known—it leads to the accurate She-Leveque intermittency exponents of velocity structure functions [14]. The phenomenological work of She and Leveque is also of great physical appeal, once it places vortex filaments as a fundamental ingredient in the production of intermittency.

We are interested, in this work, to know what the log-Poisson model may tell us about the profiles of velocity-gradient pdfs. We deal here with two sets of probability distribution functions (pdfs) for flows associated to different

Reynolds numbers. One of them is obtained from an atmospheric surface layer experiment [15–17] and the other from a direct numerical simulation (DNS) of homogeneous and isotropic turbulence [18]. The underlying motivation in this choice of systems is to show that numerical low/moderate Reynolds number results can be useful in the modeling of flows that cannot be directly simulated (even in a foreseeable future). Exactly, the same claim was put forward in a previous letter [19], where, despite the force of evidence, lacked some phenomenological basis, which—then—we develop here. We find that a bridge between low and high Reynolds number pdfs can be built within the framework of the log-Poisson model [20].

This paper is organized as follows. In Sec. II, we briefly review the multiplicative cascade models, introduce the log-Poisson model, and compute hyperflatness factors of velocity-gradient fluctuations, comparing them to recent estimates. Two relevant theorems related to velocity-gradient pdfs are also established. In Sec. III, we present the experimental and numerical data that were analyzed. In Sec. IV, the experimental and the numerical velocity gradients are closely matched with the help of a Monte Carlo procedure based on the theorems of Sec. II. In Sec. V, we summarize our results and point out directions of further research.

II. VELOCITY-GRADIENT STATISTICS**A. Multiplicative cascade models**

In the multiplicative cascade models [4], one assumes that energy flows from the integral scale L to the dissipative scale η through a number of “quantum” steps associated to eddies of sizes $L, L/a, L/a^2, \dots$, where $a > 1$ is an arbitrary rescaling factor. At length scale $\ell_m \equiv L/a^m$, the fluctuating energy-transfer rate is defined as

$$\epsilon_m = \epsilon_0 W_1 W_2 \dots W_m, \quad (2.1)$$

where the W 's are positive-independent random variables, with unit expectation value $\langle W \rangle = 1$, so that the mean energy-transfer rate is conserved along the cascade process, i.e., $\langle \epsilon_m \rangle = \epsilon_0$. The scaling behavior of velocity structure functions $S_q(r) \equiv \langle (\delta v)^q \rangle$ is then derived with the help of Kolmogorov's

refined similarity hypothesis, which postulates that fluctuations of δv at scale ℓ_m have the same moments (up to constant numerical factors) as $(\epsilon_m \ell_m)^{1/3}$.

Analogous phenomenological arguments can be put forward to deal with the case of velocity derivatives—generically denoted in the following by ∂v . The essential idea is to assume that spatial fluctuations of the velocity field are smooth at the dissipative scale and, therefore,

$$\partial v \sim \frac{\delta v_\eta}{\eta} \sim (\epsilon_\eta)^{1/3} \eta^{-2/3}, \quad (2.2)$$

where, above, δv_η is the velocity increment defined at length scale η . One may write based on purely dimensional grounds, $\eta \sim (\nu^3 / \epsilon_\eta)^{1/4}$. Thus, substituting the latter on Eq. (2.2), we get

$$\partial v \sim \sqrt{\epsilon_\eta / \nu}, \quad (2.3)$$

a statistical correspondence not unknown to the previous literature [21]. A more interesting formulation of the refined similarity hypothesis is given in terms of probability distributions. As it is clear, velocity-gradient pdfs can be always written as

$$\rho(\partial v) = \int_0^\infty d\epsilon \rho_1(\epsilon) \rho_2(\partial v | \epsilon), \quad (2.4)$$

where $\rho_2(\partial v | \epsilon)$ is the velocity-gradient pdf conditioned on the energy-transfer rate $\epsilon_\eta = \epsilon$ and $\rho_1(\epsilon)$ is the pdf associated to events, which have $\epsilon_\eta = \epsilon$. The refined similarity hypothesis is then the statement that at large Reynolds numbers,

$$\rho_2(\partial v | \epsilon) = \sqrt{\nu / \epsilon} F(\sqrt{\nu / \epsilon} \partial v), \quad (2.5)$$

where $F(\cdot)$ is a universal (Reynolds number independent) function of its argument. In fact, taking Eqs. (2.4) and (2.5), it is not difficult to show, in agreement with Eq. (2.3), that

$$\langle (\partial v)^q \rangle = C_q \langle (\epsilon_\eta / \nu)^{q/2} \rangle, \quad (2.6)$$

where

$$C_q = \int_{-\infty}^\infty dx x^q F(x). \quad (2.7)$$

It is worth noting that the form of the universal functions $F(x)$ for the case of velocity differences has been the subject of experimental research [22,23]. As a first approximation, $F(x)$ turns to have a Gaussian profile, but one expects asymmetric corrections to be relevant in the problem of longitudinal structure functions, due to their nonvanishing skewness

B. Log-Poisson model

In the log-Poisson model [12,13], one writes down the energy-transfer rate factors as

$$W = a^{\mu - m}, \quad (2.8)$$

where $a = 3/2$, $\mu = 2/3$, and $m \geq 0$ is a Poisson random variable, with expectation value

$$c = \frac{a\mu}{a-1} \ln a = 2 \ln \left(\frac{3}{2} \right). \quad (2.9)$$

In order to cope with velocity-gradient fluctuations, it is necessary to set up in the first place the total number N of cascade steps associated to the turbulent flow under scrutiny. In other words, we would like to find N , such that $\eta = L/a^N$. We stress that the multiplicative cascade description addressed here is far from being a rigorous framework since we take the Kolmogorov scale $\eta \sim \epsilon_\eta^{-1/4}$ to be a fluctuating quantity. Thus, N should be defined, necessarily, from some averaging procedure. We adopt a simple prescription based on the definition of the Reynolds number as [4]

$$R_e = \frac{L^{4/3} \epsilon_0^{1/3}}{\nu} = \left[\left\langle \left(\frac{L}{\eta} \right)^4 \right\rangle \right]^{1/3} \equiv a^{(4/3)N}. \quad (2.10)$$

Therefore, we find

$$N = \frac{3}{4} \log_a R_e. \quad (2.11)$$

An alternative and useful expression for N can be given in terms of the Taylor-based Reynolds number R_λ , which follows by taking the homogeneous isotropic result $R_\lambda = \sqrt{15} R_e$ [4],

$$N = \frac{6}{4} \log_a R_\lambda - \frac{3}{4} \log_a 15. \quad (2.12)$$

C. Hyperflatness factors

As a direct application of the log-Poisson model, we compute the Reynolds-dependent velocity-gradient hyperflatness factors defined as

$$H_q(R_\lambda) \equiv \frac{\langle (\partial v)^q \rangle}{\langle (\partial v)^2 \rangle^{q/2}}. \quad (2.13)$$

A straightforward manipulation of Eq. (2.13), taking into account Eqs. (2.1), (2.6), and (2.8), gives

$$H_q(R_\lambda) = \frac{C_q}{C_2^{q/2}} \left\langle \left(\frac{\epsilon_\eta}{\epsilon_0} \right)^{q/2} \right\rangle = \frac{C_q}{C_2^{q/2}} \langle W^{q/2} \rangle^N = A_q R_\lambda^{\alpha_q}, \quad (2.14)$$

where

$$A_q = \frac{C_q}{C_2^{q/2}} 15^{-\alpha_q/2}, \quad (2.15)$$

with

$$\alpha_q = \frac{3}{2} \log_a \langle W^{q/2} \rangle = \frac{3}{4} q \mu - \frac{3}{2} \frac{a\mu}{a-1} [1 - a^{-q/2}]. \quad (2.16)$$

In particular, the skewness and flatness coefficients predicted by Eq. (2.16) are $\alpha_3 \approx 0.13$ and $\alpha_4 = 1/3$, respectively. A good agreement is found from the recent account of Ishihara *et al.* [24], which yields $\alpha_3 = 0.11 \pm 0.01$ and $\alpha_4 = 0.34 \pm 0.03$.

If R_A and R_B are Taylor-based Reynolds numbers, respectively, associated to flows with N_A and N_B cascade steps, then Eq. (2.14) implies that

$$\frac{H_q(R_A)}{H_q(R_B)} = \langle W^{q/2} \rangle^{N_A - N_B}, \quad (2.17)$$

and, thus, taking into account Eq. (2.16),

$$N_A - N_B = \frac{3}{2\alpha_q} \log_a \frac{H_q(R_A)}{H_q(R_B)}, \quad (2.18)$$

a quantity that measures the “distance” between cascades, going to play an important role in Sec. IV.

D. Velocity-gradient PDFs

We are interested to explore further consequences of the log-Poisson cascade picture in the setting of velocity-gradient pdfs. In order to render the exposition more systematic, we introduce two important results in the form of theorems.

Theorem 1. Let $\sigma^2 \equiv \langle (\partial v)^2 \rangle$. The standardized pdf $\tilde{\rho}(\partial v) \equiv \sigma \rho(\sigma \partial v)$ has a universal profile at fixed R_λ .

Proof. We obtain, from Eqs. (2.4) and (2.5),

$$\begin{aligned} \tilde{\rho}(\partial v) &= \sigma \rho(\sigma \partial v) \\ &= \sigma \int_0^\infty d\epsilon \rho_1(\epsilon) \sqrt{\nu/\epsilon} F(\sigma \sqrt{\nu/\epsilon} \partial v) \\ &= \nu \sigma^2 \int_0^\infty d\epsilon \rho_1(\nu \sigma^2 \epsilon) \sqrt{1/\epsilon} F(\sqrt{1/\epsilon} \partial v). \end{aligned} \quad (2.19)$$

Our task, thus, is to show that $\nu \sigma^2 \rho_1(\nu \sigma^2 \epsilon)$ is indeed universal. Since the sum of Poisson random variables is also a Poisson random variable, Eqs. (2.1) and (2.8) lead, for a cascade with N steps, to

$$\epsilon_\eta = \epsilon_0 a^{N\mu - m}, \quad (2.20)$$

where m is a Poisson random variable with expectation value Nc . We may write, thus,

$$\rho_1(\epsilon) = \sum_{m=0}^\infty \frac{(Nc)^m e^{-Nc}}{m!} \delta(\epsilon - \epsilon_0 a^{N\mu - m}). \quad (2.21)$$

Now, according to Eq. (2.6) we write the variance of ∂v as $\sigma^2 = \epsilon_0 C_2 / \nu$ and, therefore, find

$$\nu \sigma^2 \rho_1(\nu \sigma^2 \epsilon) = C_2 \sum_{m=0}^\infty \frac{(Nc)^m e^{-Nc}}{m!} \delta(C_2 \epsilon - a^{N\mu - m}), \quad (2.22)$$

which, in fact, ultimately depends only on R_λ . ■

Theorem 2. Let A and B denote flows with Taylor-based Reynolds numbers R_A and R_B associated to log-Poisson cascades with N_A and N_B steps and velocity-gradient pdfs

$$\begin{aligned} \rho_A(\partial v) &= \int_0^\infty d\epsilon \rho_1^A(\epsilon) \sqrt{\nu/\epsilon} F(\sqrt{\nu/\epsilon} \partial v), \\ \rho_B(\partial v) &= \int_0^\infty d\epsilon \rho_1^B(\epsilon) \sqrt{\nu/\epsilon} F(\sqrt{\nu/\epsilon} \partial v). \end{aligned} \quad (2.23)$$

It follows that

$$\tilde{\rho}_A(\partial v) = \int_0^\infty \frac{dx}{x} K(x) \tilde{\rho}_B\left(\frac{\partial v}{x}\right), \quad (2.24)$$

where $K(x)$ is the pdf of the random variable

$$x = a^{1/2(N_A - N_B)\mu - m/2}, \quad (2.25)$$

which, on its turn, is defined in terms of m , a random Poisson variable with expectation value $(N_A - N_B)c$.

Proof. A proof follows by direct substitution of the explicit form of $K(x)$ in Eq. (2.24). Defining $g = a^{N\mu/2}$, with $N = N_A - N_B$, we may write

$$K(x) = \sum_{m=0}^\infty \frac{(Nc)^m e^{-Nc}}{m!} \delta(x - ga^{-m/2}). \quad (2.26)$$

Using Eqs. (2.22) and (2.26), we obtain, for the right-hand side of Eq. (2.24),

$$\begin{aligned} \int_0^\infty \frac{dx}{x} K(x) \tilde{\rho}_B\left(\frac{\partial v}{x}\right) &= \int_0^\infty \frac{dx}{x} \sum_{m=0}^\infty \frac{(Nc)^m e^{-Nc}}{m!} \delta(x - ga^{-m/2}) \\ &\quad \times \int_0^\infty d\epsilon \nu \sigma_B^2 \rho_1^B(\nu \sigma_B^2 \epsilon) \\ &\quad \times \sqrt{1/\epsilon} F(\sqrt{1/\epsilon} \partial v/x) \\ &= C_2 \int_0^\infty \frac{dx}{x} \int_0^\infty d\epsilon \sum_{m=0}^\infty \sum_{m'=0}^\infty \\ &\quad \times \frac{(Nc)^m e^{-Nc}}{m!} \frac{(N_B c)^{m'} e^{-N_B c}}{m'!} \\ &\quad \times \delta(x - ga^{-m/2}) \delta(C_2 \epsilon - a^{N_B \mu - m'}) \\ &\quad \times \sqrt{1/\epsilon} F(\sqrt{1/\epsilon} \partial v/x). \end{aligned} \quad (2.27)$$

Performing the substitution $\epsilon \rightarrow \epsilon/x^2$ in Eq. (2.27) and subsequently integrating over x , we get

$$\begin{aligned} C_2 \int_0^\infty d\epsilon \sum_{m=0}^\infty \sum_{m'=0}^\infty \frac{(Nc)^m (N_B c)^{m'} e^{-N_A c}}{m! m'!} \\ \times \delta(C_2 \epsilon - g^2 a^{N_B \mu - m - m'}) \sqrt{1/\epsilon} F(\sqrt{1/\epsilon} \partial v). \end{aligned} \quad (2.28)$$

Define, now, $p = m + m'$, so that Eq. (2.28) becomes

$$\begin{aligned} C_2 \int_0^\infty d\epsilon \sum_{p=0}^\infty \sum_{m=0}^p \frac{(Nc)^m (N_B c)^{m-p} e^{-N_A c}}{m! (m-p)!} \\ \times \delta(C_2 \epsilon - g^2 a^{N_B \mu - p}) \sqrt{1/\epsilon} F(\sqrt{1/\epsilon} \partial v) \\ = C_2 \int_0^\infty d\epsilon \sum_{p=0}^\infty \frac{(N_A c)^p e^{-N_A c}}{p!} \\ \times \delta(C_2 \epsilon - a^{N_A \mu - p}) \sqrt{1/\epsilon} F(\sqrt{1/\epsilon} \partial v) \\ = \tilde{\rho}_A(\partial v). \end{aligned} \quad (2.29)$$

■

In view of theorem 2, we can devise a straightforward Monte Carlo integration procedure in order to relate velocity-gradient pdfs defined at different Reynolds numbers. In fact, if $x > 0$ and y are random variables of two independent stochastic process, described, respectively, by pdfs $K(x)$ and $\tilde{\rho}(y)$, then the random variable $z=xy$ is given by the pdf

$$\begin{aligned} \langle \delta(z - xy) \rangle_{x,y} &= \int dx dy K(x) \tilde{\rho}(y) \delta(z - xy) \\ &= \int_0^\infty \frac{dx}{x} K(x) \tilde{\rho}\left(\frac{z}{x}\right) \\ &= \tilde{\rho}(z), \end{aligned} \quad (2.30)$$

where we have used Eq. (2.24) in the last equality above. We have found that it is greatly advantageous to use Monte Carlo integration, instead of more traditional numerical methods, a fact probably due to the poor convergence properties of the latter in our particular problem.

III. ATMOSPHERIC SURFACE LAYER EXPERIMENT

Atmospheric surface layer velocity fluctuations were studied over a grass-covered flat surface in the Sils-Maria valley, Switzerland [15], a place which hosts reasonably stable winds. The results reported in this work correspond to measurements of all of the nine components of the velocity-gradient tensor performed in a tower 3.0 m high. The velocity signal was recorded at a sampling rate of 10 KHz (which was high enough to resolve the dissipative scales), with the help of a 20 hot-wire probe anemometer, specifically designed for the particularities of the field experiment.

Velocity gradients were computed without resort to the Taylor's frozen turbulence hypothesis. The Taylor-based Reynolds number of the flow estimated from the Taylor length $\lambda = \sqrt{u_1^2} / \langle (\partial_1 u_1)^2 \rangle$ is $R_\lambda = 3.4 \times 10^3$ (u_1 is the projection of the velocity fluctuations along the flow direction). We note that since the flow is somewhat anisotropic, the definition of a meaningful Taylor-based Reynolds number may be problematic. We will get back to this point in Sec. IV.

The experimental velocity-gradient pdfs are shown Fig. 1. We find a good (to within error bars) collapse of standardized pdfs of velocity gradients $s_{ij} = \partial_j u_i$ with $i \neq j$. Due to anisotropy effects in the surface layer, however, there is no collapse for the standardized pdfs of diagonal components s_{ii} , and we have discarded the curves for s_{22} and s_{33} assuming, as a working hypothesis to be tested *a posteriori*, that isotropic results would correspond to the set $\{s_{11}, s_{ij}\}$, with $i \neq j$.

The central aim of this work is to model the pdfs depicted in Fig. 1 using DNS results for homogeneous and isotropic turbulence obtained at the considerably lower Taylor-based Reynolds number $R_\lambda = 240$ (the numerical data correspond to simulations discussed in Ref. [18]). The corresponding DNS velocity-gradient pdfs are shown in Fig. 2. As it follows from this figure, the pdfs collapse into two distinct groups associated to the diagonal and nondiagonal components of the velocity-gradient tensor s_{ij} . Of course, we do not expect that the pdfs given in Fig. 2 yield a direct fitting to the ones of

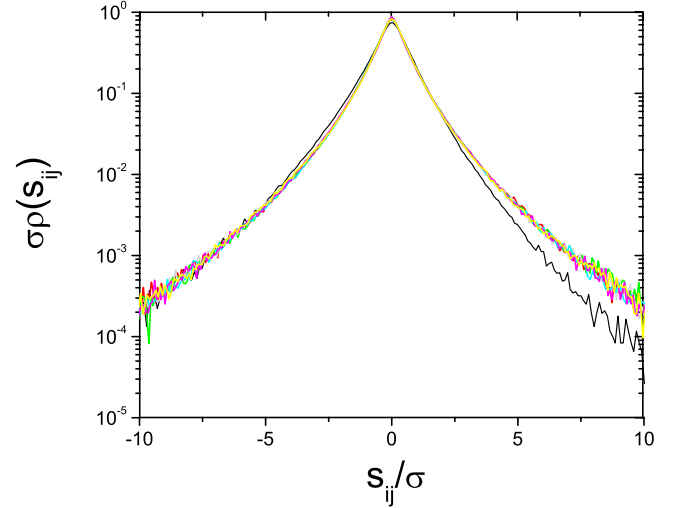


FIG. 1. (Color online) Experimental velocity-gradient pdfs for atmospheric surface layer flow with $R_\lambda = 3.4 \times 10^3$. Black (darker) line: s_{11} ; colored (lighter) lines: s_{ij} , with $i \neq j$.

Fig. 1—there is a clear discrepancy as shown in Figs. 3 and 4.

IV. MONTE CARLO PDF RECONSTRUCTION

Our computational strategy is to consider the experimental ($R_\lambda = 3.4 \times 10^3$) and the numerical ($R_\lambda = 240$) flows discussed in Sec. III as the systems A and B, respectively, of theorem 2. An important parameter here is the cascade distance $N_A - N_B$ of these flows. This quantity can be computed by measuring the flatness factors H_4 of flows A and B and using them as input parameters in Eq. (2.18). From the pdfs of s_{11} , we get

$$H_4(A) = 11.5,$$

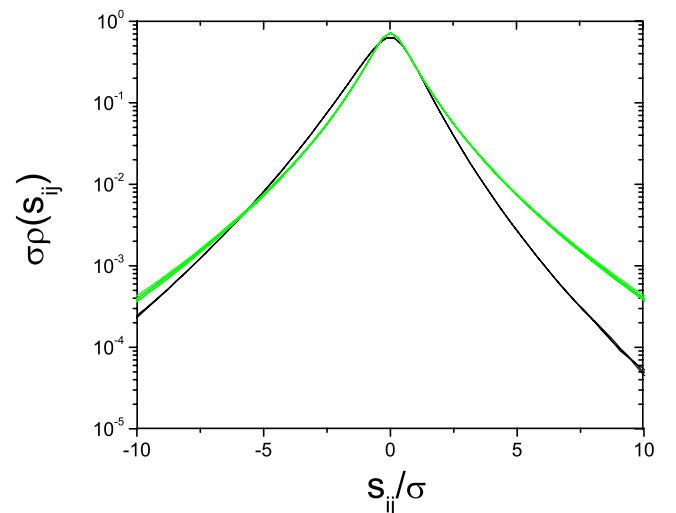


FIG. 2. (Color online) Numerical velocity-gradient pdfs for homogeneous isotropic turbulence with $R_\lambda = 240$. Black lines: diagonal components s_{ii} ; green (light gray) lines: nondiagonal components s_{ij} .

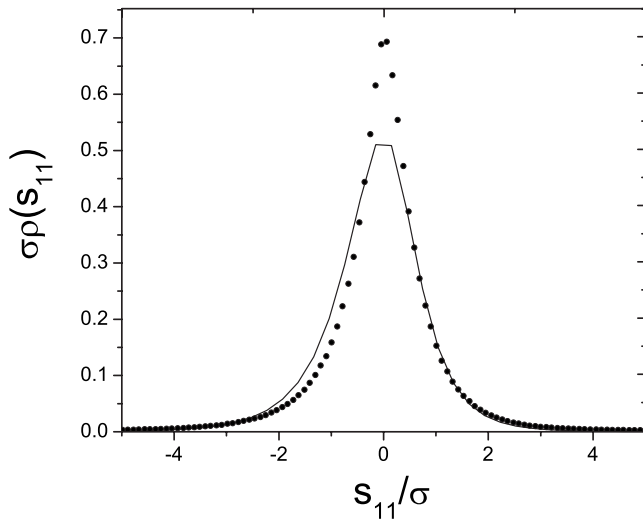


FIG. 3. Comparison between the numerical ($R_\lambda=240$; solid line) and the experimental ($R_\lambda=3.4 \times 10^3$; dots) pdfs of s_{11} .

$$H_4(B) = 6.6. \quad (4.1)$$

Therefore, using Eq. (2.18), with $\alpha_4=1/3$, we find

$$N_A - N_B = \frac{9}{2} \log_{3/2} \left(\frac{11.5}{6.6} \right) = 6.16. \quad (4.2)$$

Due to the discrete structure of the cascade in the multiplicative models, we take $N_A - N_B = 6$ in the following considerations.

Using a random Poisson variable generator as the one given in Ref. [25], it is straightforward to establish a stochastic process with random variable given by Eq. (2.25). On the other hand, in order to generate a stochastic process with random variable described by the numerical pdf of s_{11} , we proceed in two steps. First, we define an accurate polynomial fitting to the $\log_{10} \tilde{\rho}_B(s_{11})$ profile; second, the polynomial analytical distribution just obtained is used in a Monte Carlo accept-reject algorithm [26], which produces random vari-

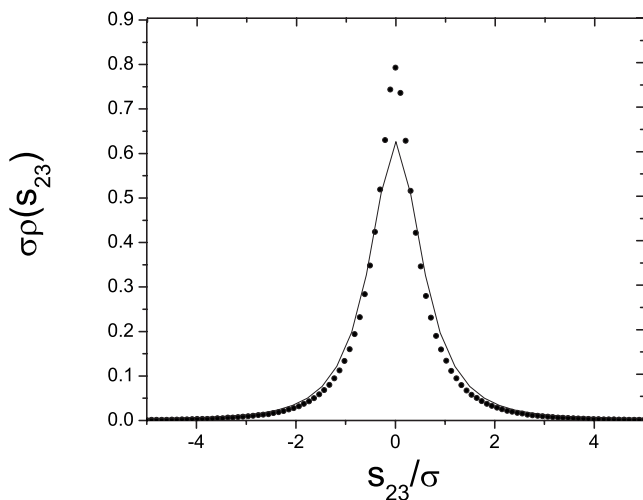


FIG. 4. Comparison between the numerical ($R_\lambda=240$; solid line) and the experimental ($R_\lambda=3.4 \times 10^3$; dots) pdfs of s_{23} .

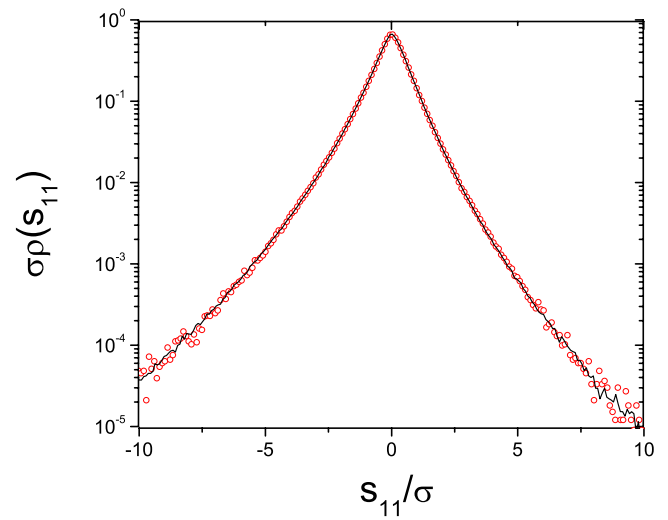


FIG. 5. (Color online) The numerically reconstructed pdf of s_{11} (black solid line) is compared to the experimental pdf (red circles).

ables distributed according to $\tilde{\rho}_B(s_{11})$. Analogous computations are performed for the numerical pdfs of s_{23} , which are taken as a representative of the nondiagonal components of the velocity-gradient tensor. By multiplying the stochastic processes associated to the Poisson and the numerical pdfs, we get standardized pdfs, which would hopefully fit the experimental curves. We have taken a process with 2×10^7 elements. In fact, an excellent agreement is attained from the Monte Carlo reconstructed pdfs, as shown in Figs. 5 and 6. A comparison between the modeled and the experimental pdfs is also shown in Figs. 7 and 8 in linear scales to be contrasted to Figs. 3 and 4.

It is important to emphasize that the remarkable fittings shown in Figs. 5–8, between the numerical and experimental pdfs for the set $\{s_{11}, s_{ij}\}$, are obtained from the mapping determined by the single parameter $N_A - N_B$ provided by the fluctuations given by Eq. (2.25). This constitutes a strong

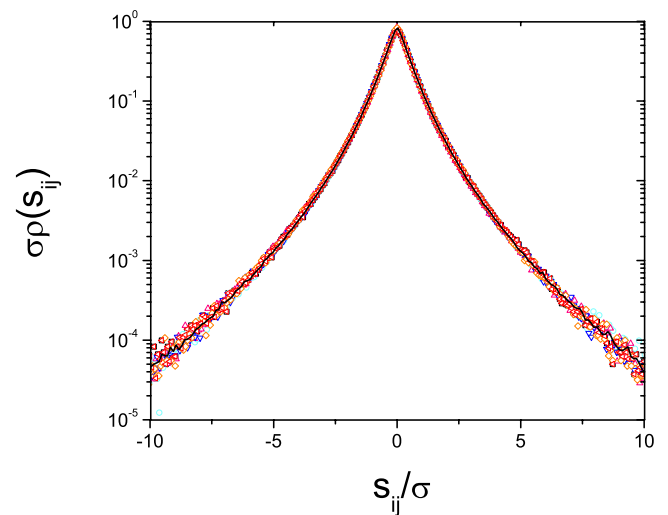


FIG. 6. (Color online) The numerically reconstructed pdf of s_{23} (black solid line) is compared to the experimental pdfs of s_{ij} , with $i \neq j$ (colored symbols).

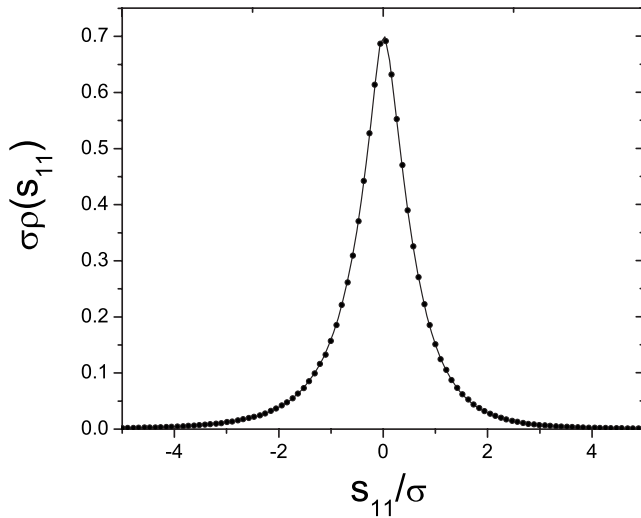


FIG. 7. The numerically reconstructed pdf of s_{11} (solid line) is compared to the experimental pdf (dots) in linear scales.

evidence for the existence of an underlying log-Poisson cascade process. We note, furthermore, that the agreement between modeled and experimental pdfs would be not so good if the experimental pdfs of s_{22} or s_{33} were chosen in place of the one for s_{11} . The present method, thus, has the heuristic potential to address issues of isotropy in boundary layer flows.

A further application of our results is the definition of an *effective* Reynolds number \bar{R}_λ for the atmospheric surface turbulent flow, taking the more controlled Reynolds number of the DNS as a standard. We write, according to Eq. (2.14),

$$\bar{R}_\lambda = 240 \times \left(\frac{11.5}{6.6} \right)^3 \approx 1.2 \times 10^3. \quad (4.3)$$

It was noted, in Ref. [15], that the rough estimate $R_\lambda = 3.4 \times 10^3$ displaces the point $(R_\lambda, H_4) = (3.4 \times 10^3, 11.5)$ out of the empirical curve well modeled $H_4 \sim R_\lambda^{\alpha_4}$. However, we

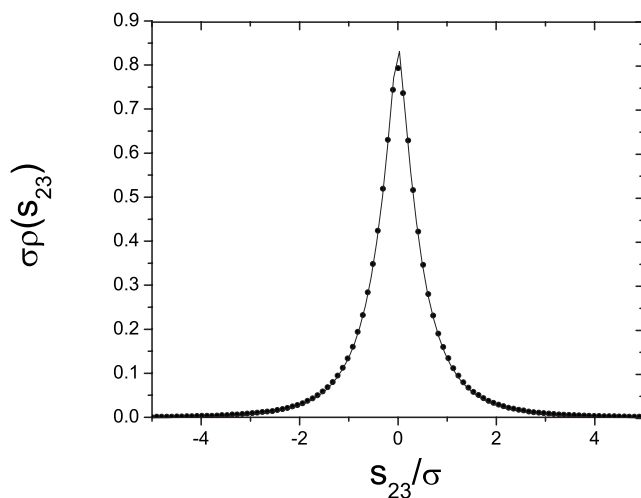


FIG. 8. The numerically reconstructed pdf of s_{23} is compared to the experimental pdf (dots) in linear scales.

find that if the alternative value (4.3) is used instead of $R_\lambda = 3.4 \times 10^3$, then the point (R_λ, H_4) gets closer to the usual curve of flatness.

V. CONCLUSIONS

We have used the log-Poisson model of the turbulent cascade to get the pdfs of velocity-gradient fluctuations of a high Reynolds turbulent atmospheric flow. The excellent fittings are achieved by means of a Monte Carlo integration procedure and the use of standard pdfs obtained in a lower Reynolds number DNS. Our results indicate that non-Gaussianity and anomalous scaling of scale-dependent observables can be seen as different manifestations of intermittency that can be approached within a unified framework. Actually, this point of view has been formerly pursued along the multifractal description of intermittency [27], with modest success in the quality of pdf fittings, nevertheless, the fact that they are dependent on a large number of free parameters.

As a natural application of our methodology, we have found a way to (i) select isotropy sectors of the velocity-gradient tensor in boundary layer flows and (ii) unambiguously define effective Taylor-based Reynolds numbers in the presence of anisotropy. These results can be of considerable interest in the study of anisotropy effects in turbulent boundary layers. It is also likely that the same ideas can be extended to the case of free shear turbulence.

An interesting question is how low can be the DNS Reynolds number, while still leading to good velocity-gradient pdf fittings for higher Reynolds number flows, along the lines discussed in Sec. IV. An investigation of this matter could throw some light on the problem of extended self-similarity [28]. Also, we wonder if correlation effects in the velocity-gradient time series could be modeled in similar ways. A promising direction here would be to link the Fokker-Planck approach to turbulent time series [29] with the log-Poisson cascade model.

It is clear that the multiplicative cascade picture is worth as a phenomenological construction if a consistent meaning can be given to concepts such as the inertial range, local cascade, and the universality of velocity structure exponents. However, recent work [30] on the scaling behavior of velocity structure functions suggests that inertial and dissipative range fluctuations could be coupled in a bidirectional way. It has been found in [30] that the scaling exponents measured in the inertial range are changed if strong dissipative events are discarded in the averaging procedure, indicating a “flow of influence” from the small to the large scales.

In order to address further related studies, we note that a possible solution to these puzzling observations, saving the essence of the multiplicative cascade phenomenology, would rely on the usual definition of the energy dissipation rate ϵ_m as the local dissipation rate averaged over volumes with linear sizes on the order of $\ell_m = L/a^m$. Since the energy dissipation rate is long range correlated, it is likely that events, which have strong local dissipation rates, turn to be correlated with strong events in the above (inertial range averaged) sense.

ACKNOWLEDGMENTS

We thank the U.S.-Israel Binational Foundation and the Israel Science Foundation (M.K. and A.T.) and CAPES,

CNPq, and FAPERJ (L.M. and R.M.P.) for support. We are most indebted to P. K. Yeung for his kind attention in providing us with DNS data and to F. S. Amaral for interesting discussions.

-
- [1] G. K. Batchelor and A. A. Townsend, Proc. R. Soc. London, Ser. A **199**, 238 (1949).
- [2] A. N. Kolmogorov, Dokl. Akad. Nauk SSSR **30**, 9 (1941); Proc. R. Soc. London, Ser. A **434**, 9 (1991).
- [3] A. N. Kolmogorov, Dokl. Akad. Nauk SSSR **32**, 16 (1941); Proc. R. Soc. London Ser. A **434**, 15 (1991).
- [4] U. Frisch, *Turbulence: The Legacy of A.N. Kolmogorov* (Cambridge University Press, Cambridge, 1995).
- [5] U. Frisch, Proc. R. Soc. London, Ser. A **434**, 89 (1991).
- [6] F. Anselmet, Y. Gagne, E. J. Hopfinger, and R. A. Antonia, J. Fluid Mech. **140**, 63 (1984).
- [7] A. N. Kolmogorov, J. Fluid Mech. **13**, 82 (1962).
- [8] A. M. Oboukhov, J. Fluid Mech. **13**, 77 (1962).
- [9] S. Kida, J. Phys. Soc. Jpn. **60**, 5 (1991); Fluid Dyn. Res. **8**, 135 (1991).
- [10] A. Tsinober, *An Informal Introduction to Turbulence* (Kluwer Academic Press, Netherlands, 2001).
- [11] J. Bec and K. Khanin, Phys. Rep. **447**, 1 (2007).
- [12] B. Dubrulle, Phys. Rev. Lett. **73**, 959 (1994).
- [13] Z.-S. She and E. C. Waymire, Phys. Rev. Lett. **74**, 262 (1995).
- [14] Z.-S. She and E. Leveque, Phys. Rev. Lett. **72**, 336 (1994).
- [15] G. Gulitski, M. Kholmyansky, W. Kinzelbach, B. Lüthi, A. Tsinober, and S. Yorish, J. Fluid Mech. **589**, 57 (2007).
- [16] G. Gulitski, M. Kholmyansky, W. Kinzelbach, B. Lüthi, A. Tsinober, and S. Yorish, J. Fluid Mech. **589**, 83 (2007).
- [17] G. Gulitski, M. Kholmyansky, W. Kinzelbach, B. Lüthi, A. Tsinober, and S. Yorish, J. Fluid Mech. **589**, 103 (2007).
- [18] D. Donzis, P. K. Yeung, and K. Sreenivasan, Phys. Fluids **20**, 045108 (2008).
- [19] M. Kholmyansky, L. Moriconi, and A. Tsinober, Phys. Rev. E **76**, 026307 (2007).
- [20] The use of log-normal statistics in Ref. [19] is now understood to be just a good approximation to the improved picture provided by the log-Poisson model.
- [21] J. C. Wyngaard and H. Tennekes, Phys. Fluids **13**, 1962 (1970).
- [22] Y. Gagne, M. Marchand, and B. Castaing, J. Phys. II **4**, 1 (1994).
- [23] A. Naert, B. Castaing, B. Chabaud, B. Htbral, and J. Peinke, Physica D **113**, 73 (1998).
- [24] T. Ishihara, Y. Kaneda, M. Yokokawa, K. Itakura, and A. Uno, J. Fluid Mech. **592**, 335 (2007).
- [25] D. Knuth, *Seminumerical Algorithms*, The Art of Computer Programming (Addison-Wesley, Reading, MA, 1981), Vol. 2.
- [26] M. E. J. Newman and G. T. Barkema, *Monte Carlo Methods in Statistical Physics* (Oxford University Press, Oxford, 2001).
- [27] R. Benzi, L. Biferale, G. Paladin, A. Vulpiani, and M. Vergasola, Phys. Rev. Lett. **67**, 2299 (1991).
- [28] R. Benzi, S. Ciliberto, R. Tripiccion, C. Baudet, F. Massaioli, and S. Succi, Phys. Rev. E **48**, R29 (1993).
- [29] J. Peinke, A. Nawoth, S. T. Lück, M. Siefert, and R. Friedrich, *Stochastic Analysis and New Insights into Turbulence*, Advances in Turbulence XI (Springer, New York, 2007).
- [30] M. Kholmyansky and A. Tsinober, Phys. Lett. A **373**, 2364 (2009).